International Journal of Geosynthetics and Ground Engineering (2020) 6:16
https://doi.org/10.1007/s40891-020-00205-2

ORIGINAL PAPER

Effect of Influencing Parameters on the Vibration Isolation Efficacy of Geocell Reinforced Soil Beds

Hasthi Venkateswarlu[1] · **A. Hegde**[1]

Received: 14 March 2020 / Accepted: 13 May 2020 / Published online: 25 May 2020

Abstract

This manuscript evaluates the effect of various influencing factors on the vibration mitigation efficiency of geocell-reinforced foundation beds. Parameters investigated include the width of geocell, depth of placement of geocell below the footing, depth of embedment of footing, infill materials, and the dynamic force level of the excitation. The effect of aforesaid parameters was studied by performing field vibration tests over the reinforced test beds of 3.6 m × 3.6 m × 1.2 m. To understand the vibration isolation efficacy, different vibration indicators, viz., displacement amplitude, peak particle velocity (PPV), and peak acceleration were evaluated. From the results, reinforcing the soil bed with geocell was found to be a worthwhile approach to control the vibration parameters. For achieving the maximum isolation, the optimum width and depth of placement of geocell were found to be $5B$ and $0.1B$ respectively. At its optimum width and depth of placement, the peak particle velocity was reduced by 50%. Similarly, it was observed that the 53% drop in the peak displacement amplitude of the foundation bed. Vibration parameters in the geocell reinforced case were found attenuated with the increase in footing embedment and modulus of infill material. On the other hand, the vibration parameters of the unreinforced and geocell reinforced cases were amplified distinctly due to the increase in dynamic excitation.

Keywords Geocell · Field vibration test · Influencing factors · Vibration parameters · Isolation efficiency

Introduction

In recent times, ground vibration sources are increasing at a rapid rate due to several manmade activities. The expansion of transit systems (both the road and railways), blasting, construction activities (dynamic compaction; piling), and the operation of heavy machines are the few examples of such activities. The intense levels of induced vibration may jeopardize the performance of old monuments, sensitive equipment, underground pipelines, and create annoyance to inhabitants living in nearby areas [1]. To reduce the adverse effects of vibration, various countermeasures were suggested in the past. Among those, isolation of ground vibration is the most common countermeasure used in the practice. It is achieved by installing the barrier at specified location along the wave transmission direction between the structure and source. Thus, the transmission of induced vibration can be modified through scattering and diffraction mechanisms. The vividly adopted wave barriers include rows of solid piles [2], gas mattresses [3], open and in-filled trenches [4–6]. Based on its location, isolation techniques have been categorized into two types namely, near field, and far-field vibration isolation. The near field isolation is aimed to attenuate the amplitude of vibration at the vibration source. Whereas, the amplitude of induced vibration is mitigated near the structure in the case of far-field vibration isolation. In the case of barrier systems, generally, the depth is larger than the horizontal dimension. It is not always practically feasible to excavate the huge quantity of soil mass in the urban areas due to instability of the soil, adjacent foundation requirements, underground water, and other issues.

On the other hand, the application of horizontal wave barriers for vibration isolation has drawn considerable attention in the recent past. These barriers can be referred as wave impedance block (WIB). The mechanism of WIB is to change the wave transmission behavior of the subsurface by including the horizontal stiffened layer [7, 8]. Till date,

✉ Hasthi Venkateswarlu
hasthi.pce16@iitp.ac.in

A. Hegde
ahegde@iitp.ac.in

[1] Department of Civil and Environmental Engineering, Indian Institute of Technology Patna, Bihta, Bihar 801106, India

theoretical research was conducted significantly to analyse the isolation behavior of WIB [9–11]. Limited studies have highlighted the isolation aspect of WIB through experimental investigation. Kratzig and Niemann [12] described the potential use of WIB as an isolation barrier for surface footing under the active and passive conditions. In accordance with the results, WIB performance was found efficient in mitigating the vertical component of induced vibration energy. Takemiya [13] examined the effect of tire shreds on the isolation behavior of honeycomb wave impedance block. From the findings, the presence of tire shreds in the cell walls resulted in the maximum dissipation of induced energy. In addition, improvement in the wave scattering behavior was observed with the increase in stiffness of cell walls. Mandal et al. [14] observed the decrease in amplitude of vibration due to the provision of stiff soil layer beneath the surface footing.

Further, the concept of reinforced earth has attained significant importance in improving the behavior of several civil engineering applications [15–20]. Saride and Dutta [21] reported the potential use of fly ash in enriching the behavior of expansive clay beds supporting the machine foundation. The soil bed reinforced with steel bars and polymeric materials found to exhibit a noticeable efficiency in mitigating the amplitude of vibration [22]. Nowadays, the inclusion of geocell reinforcement has become a prominent practice for improving the stiffness and stability of foundation beds. The potential benefits of geocell have been reported in foundations, pavements, retaining walls, buried lifelines, embankments, steep slopes, pile foundations, and landfill applications [23–32]. Overall, limited literature is available in highlighting the vibration mitigation ability of geocell reinforced foundation beds. Venkateswarlu et al. [33] stated the increase in screening efficiency of foundation bed with the insertion of geocell reinforcement. Ujjawal et al. [34] highlighted the geocell potential in arresting the lateral spreading behavior of machine induced vibration through numerical investigations. In the above-mentioned studies, width, location of a geocell mattress, and infill material were considered constant to study the vibration response.

Out of the existing literature, there is a lack of studies, which emphasize the effect of reinforcement geometry, location, and loading characteristics on the isolation effectiveness of the geocell reinforced foundation bed. In practice, these parameters can have a significant influence on the vibration isolation performance. Hence, the present study is aimed to study the influence of five major factors on vibration isolation efficacy of geocell reinforced beds. It includes the width of the geocell, depth of placement of geocell below the footing, depth of embedment of footing, infill materials, and dynamic force. A numerous field vibration tests have been performed over the unreinforced and geocell reinforced foundation beds for this purpose.

Test Materials and Specifications

Five different geo-materials and the geocell reinforcement have been used in the present investigation. The specifications of the test materials are described below.

Geo-Material Specifications

The different geo-materials used in this study are silty sand, sand, steel slag, construction and demolition waste (CDW), and aggregate (AGG). These materials were classified using the recommendations of the Unified Soil Classification System (USCS). The compaction parameters of silty sand and CDW materials were estimated through the Standard Proctor test in accordance with ASTM D698–07 [35]. Whereas, the guidelines of ASTM D4253 [36] were followed for determining the minimum and maximum densities of other geo-materials. The shear parameters of all the geo-materials were determined in accordance with ASTM D3080 [37]. Table 1 illustrates the properties of different geo-materials. The triaxial test was performed under consolidated undrained (CU) condition to evaluate the modulus of elasticity of geomaterials.

Geocell Properties

The commercially available NPA (known as a novel polymeric alloy) geocell with a 120 mm wall height was used as the reinforcement material. The nominal opening area of each pocket of the geocell was 330 mm × 150 mm. The geocell wall consisted of rhomboidal shape texture to mobilize interface friction with the infill material. The tensile load versus axial strain behavior of a geocell specimen is shown in Fig. 1. The peak tensile load capacity and failure strain of geocell were determined as 23.8 kN/m and 12.8% respectively. These parameters were evaluated using the recommendations of ISO 10319 [38]. Other specifications of the geocell are summarized in Table 2.

Field Vibration Tests

Test Setup

The schematic view of the field vibration test set up is shown in Fig. 2a. A Lazen type of mechanical oscillator was used as a source of dynamic excitation. It consists of an eccentric mass assembly to induce sinusoidal dynamic excitation. The dynamic force can be varied through adjusting the angle between eccentric masses (known as eccentric angle) using the eccentricity controller. The eccentric angle is the angle

Table 1 Properties of geo-materials

Characteristics	Property	Unit	Geo-material				
			Silty sand	Sand	Slag	CDW	AGG
Grain size	FC	%	16	2	4	5	0
	C_c	ND	10.12	1.28	1.08	4.54	1.03
	C_u	ND	22.22	2.63	6.58	47.33	1.07
	D_{50}	mm	0.38	0.45	0.6	9.3	10.7
	USCS classification	–	SM	SP	SW	GW	GP
Compaction	OMC	%	12.6	NA	NA	9	NA
	γ_{dmin}	kN/m^3	14.5	16.5	17.2	15.8	15.3
	γ_{dmax}	kN/m^3	17.9	18.6	18.9	19.3	17.5
Strength parameters	φ	(°)	32	36	39	41	49
	c	kN/m^2	2	0	0	12	0
	E	MPa	28.3	32	40	48	60

FC fines content, C_c curvature coefficient, C_u uniformity coefficient, D_{50} medium particle size, *OMC* optimum moisture content, γ_{dmin} minimum dry density, γ_{dmax} maximum dry density, φ angle of shearing resistance, *c* cohesion, *E* elastic modulus, ND non dimensional, NA not applicable

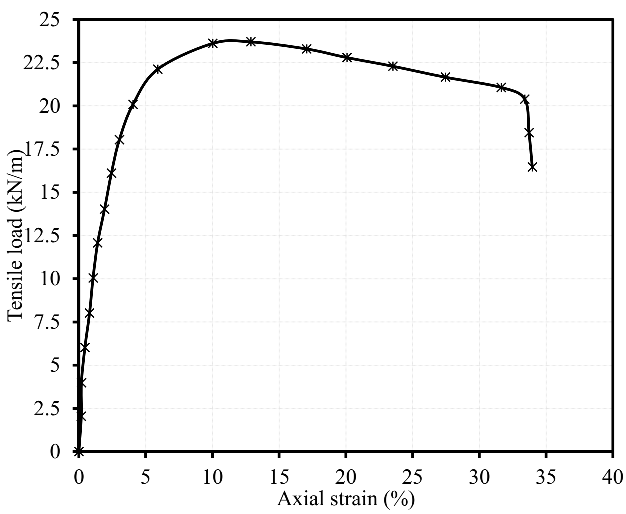

Fig. 1 Tensile load vs strain response of the geocell reinforcement

maintained by eccentric distance (*e*) with the axis of rotation [39]. The following relation can be used to quantify the total unbalanced force (X_0) generated by the oscillator.

$$X_0 = 2m_e e\omega^2$$
$$X_0 = m_0 e\omega^2 \quad (\because 2m_e = m_0) \tag{1}$$

where m_e is the mass of an individual rotating element, ω is the angular velocity, *e* denotes the eccentric distance, and m_0 indicates the total mass of the rotating elements. Further, the vertical dynamic force acting on the concrete footing is calculated using,

$$X_d = X_0 \sin\left(\frac{\theta}{2}\right) \tag{2}$$

where X_d represents the total vertical dynamic force, and θ denotes the eccentric angle. For a particular oscillator, m_0 and *e* will be constant. Thus, the induced vertical dynamic force is proportional to θ, and the working frequency of the oscillator. The mechanical oscillator was fixed over the concrete block. For convenience, the concrete block has been mentioned as a model footing in the leftover part of the manuscript. The length, width, and depth of the footing were 600 mm, 600 mm, and 500 mm, respectively.

A DC motor with 6 HP capacity was utilized to run the oscillator with the help of a flexible shaft. The operating speed of the motor was recorded and maintained using the speed control device. It quantifies the working frequency in terms of RPM with the assistance of a non-contact speed sensor. The sensing portion of the sensor was fixed at the proximity of rotating shaft. The maximum sensing frequency range of the sensor used in this study was 10,000 RPM. Total, three types of data acquisition system (DAQ) were used for recording the different vibration parameters. The micro electrical mechanical system (MEMS) type accelerometers were employed to record the vertical mode of acceleration. These are popularly used for recording the acceleration response with respect to a particular axis with high precision. A 12-channel DAQ was used for digitizing the output data of accelerometers. It consists of digital to analog converter (DAC) for supporting the sampling rates of frequency varying from 1 Hz to 25.6 kHz. At a selected frequency, peak acceleration was recorded for 150 s. The computerized program PULSE Lab shop was used for monitoring the accelerometer response. The recordings were analyzed using the Reflex program. The 3D geophone was used for recording the velocity response of the induced vibration. It was connected to the vibration monitoring terminal. The PPV and acceleration were recorded to understand the

Table 2 Characteristics of the geocell reinforcement

Property	Specifications/values	Remarks
Physical parameters		
Composition of polymer	Novel polymeric alloy	Determined by the authors
Depth of geocell pocket (mm)	120	
Cell wall thickness (mm)	1.53	
Nature of cell wall surface	Perforated and textured	
Open area on the geocell surface (%)	16	
Diameter of a hole on the surface (mm)	10	
Cells count per square meter	39	
Density (g/cm^3)	0.95 (± 1.5%)	
Mechanical parameters		
Cell seam strength (*N*)	2150 (± 5%)	Provided by the manufacturer
Endurance parameters		
Coefficient of thermal expansion (ppm/°C)	< 80	
Durability to UV degradation (min)	> 400	
Oxidation induction time (min)	≥ 100	
Creep reduction factor	< 3.5	

isolation efficiency of the foundation bed at 2 m distance from the center of model footing. The parent soil located at the depth of placement of accelerometers was silty clay having a bulk density of 16.3 kN/m^3. Further, vibration meter was used to monitor the displacement amplitude at the model footing. To do so, the piezoelectric type accelerometer was employed as a sensing component. It was attached to the vibration meter. The positioning of the different sensing elements is shown in Fig. 2b.

Preparation of Unreinforced Test Bed

Using silty sand, two different types of test beds namely, unreinforced and geocell reinforced were prepared. Both the beds were prepared in a pit following the plan dimensions 3.6 m × 3.6 m and depth 1.2 m. The length and width of the test pit were chosen six times larger than the width of a model footing to minimize the boundary effects [14]. The test bed was prepared in 12 numbers of layers with each layer depth of 100 mm. The layer-wise preparation helps to sustain the uniform density in the bed [40, 41]. Prior to the preparation of the bed, air-dried soil required to prepare each layer was weighed and mixed with optimum moisture content (OMC). The wet soil mix was kept for 12 h to attain the moisture equilibrium state. The compaction was performed manually using a steel rammer by maintaining the number of blows and height of the fall. The approximate compaction effort of 594 kN-m/m^3 (i.e. compaction effort of Standard Proctor) was applied over each layer. Further, the density and water content variation of the compacted bed was studied by means of collecting the soil samples from different locations. Total, 18 numbers of samples were collected from two different depths i.e. 0.6 m and 1.2 m (nine samples from each depth) from the bottom of the bed. IS 2720–29 [42] guidelines were followed for collecting soil samples and measuring compaction characteristics of the test bed. Dry density of the test bed was found to vary between 17.23(±0.25) kN/m^3. Likewise, the moisture content variation was observed as 12.15(±0.15)%.

Preparation of Geocell Reinforced Test Bed

Figure 2a shows the schematic outlook of the geocell reinforced foundation bed. The NPA geocell was positioned and expended on the compacted soil surface. Primarily, pockets of the geocell mattress were filled with silty sand material. Cell pockets were filled in the layers of 40 mm each. The silty sand infill was compacted using Standard Proctor rammer. The density of the infilled soil was verified by collecting soil samples from different places of the geocell layer. The dry density of the infilled soil was determined to vary between 17.2 and 17.34 kN/m^3. Further, the average dry density of silty sand infill was considered as a reference for filling the geocell pockets with other materials, namely, CDW, aggregate, sand, and steel slag. The CDW and aggregate were compacted through the tamping technique.

The sand pluviation method was adopted for filling the sand and slag materials [43]. The height of fall required for achieving the target density of both the materials was determined from the trial tests. During the pluviation, aluminum cups with known volume were placed at different locations to study the density difference. Overall, the density difference among different infill materials was found less than 9%. All the necessary precautions were taken to protect the

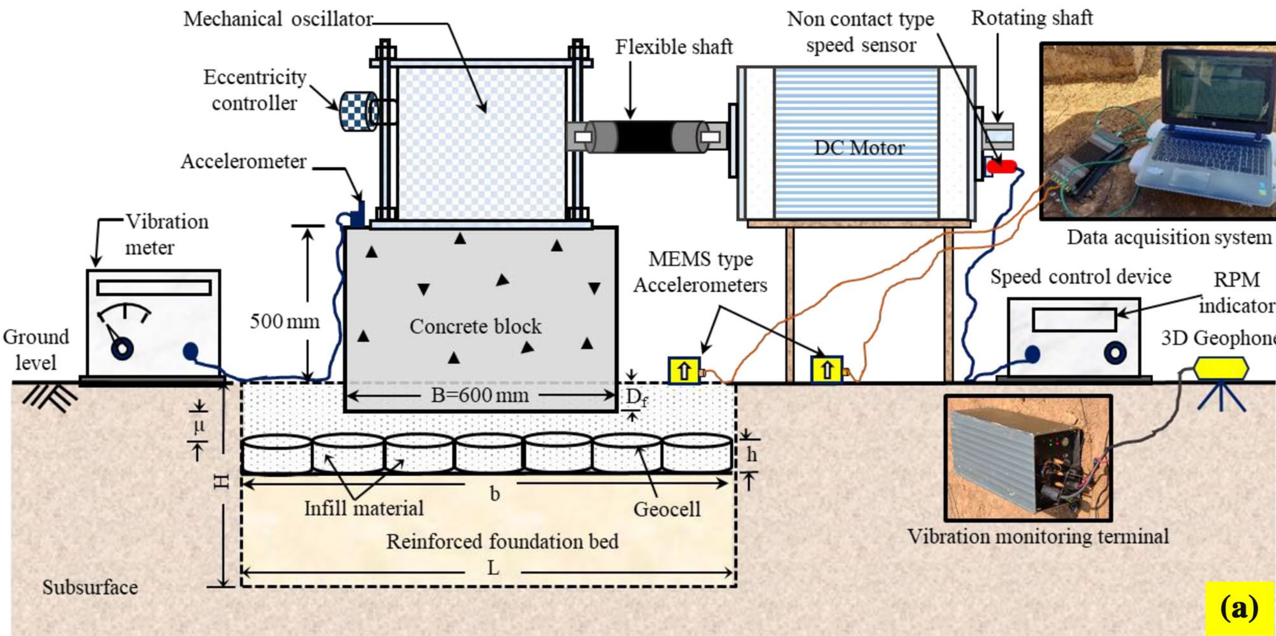

[Note: D_f is the depth of embedment of the footing; B is the width of the model footing; b is the width of the geocell mattress; μ is the depth of placement of geocell mattress below the footing; h is the height of geocell mattress; H is the depth of the foundation bed; L is the length of the foundation bed.]

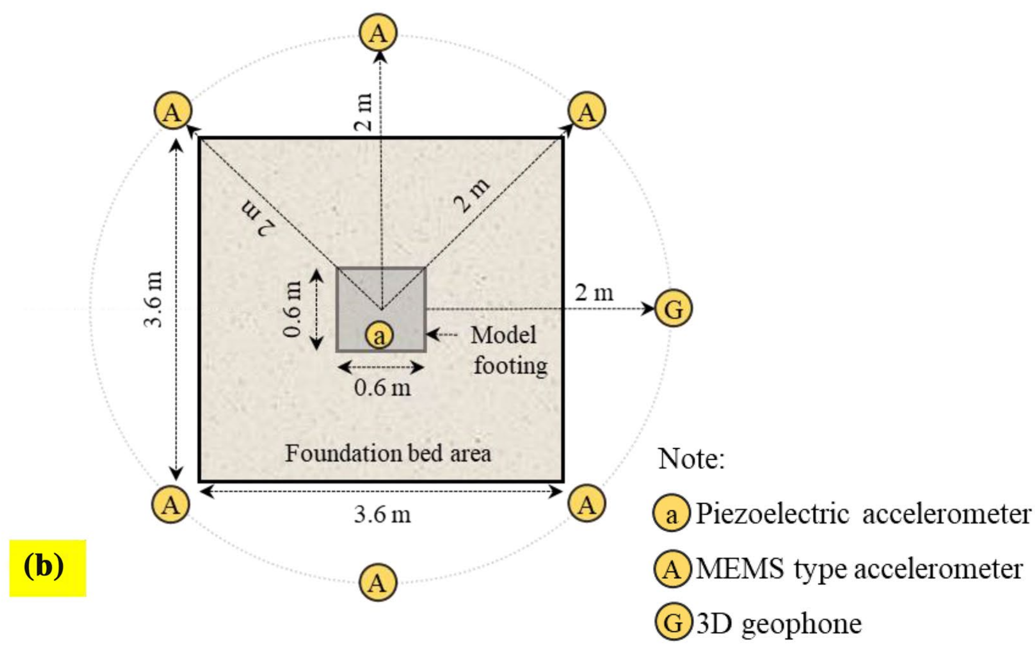

Fig. 2 Test setup: **a** schematic view of field vibration test; and **b** arrangement of sensors

geocell reinforcement from bending and distortion effects [29, 33]. Over the geocell infilled layer, the soil cover of varying thickness was provided depending on the depth of placement of geocell in a particular test. The infill material of the corresponding condition was used for providing the soil cover over the geocell composite layer.

Figure 3a–d shows the photographs conforming to the preparation of different reinforced test beds.

In addition to the tests conducted on unreinforced soil bed, four series of tests were conducted over the geocell reinforced foundation beds namely, GRFB-I, GRFB-II, GRFB-III, and GRFB-IV. The effect of the width of geocell

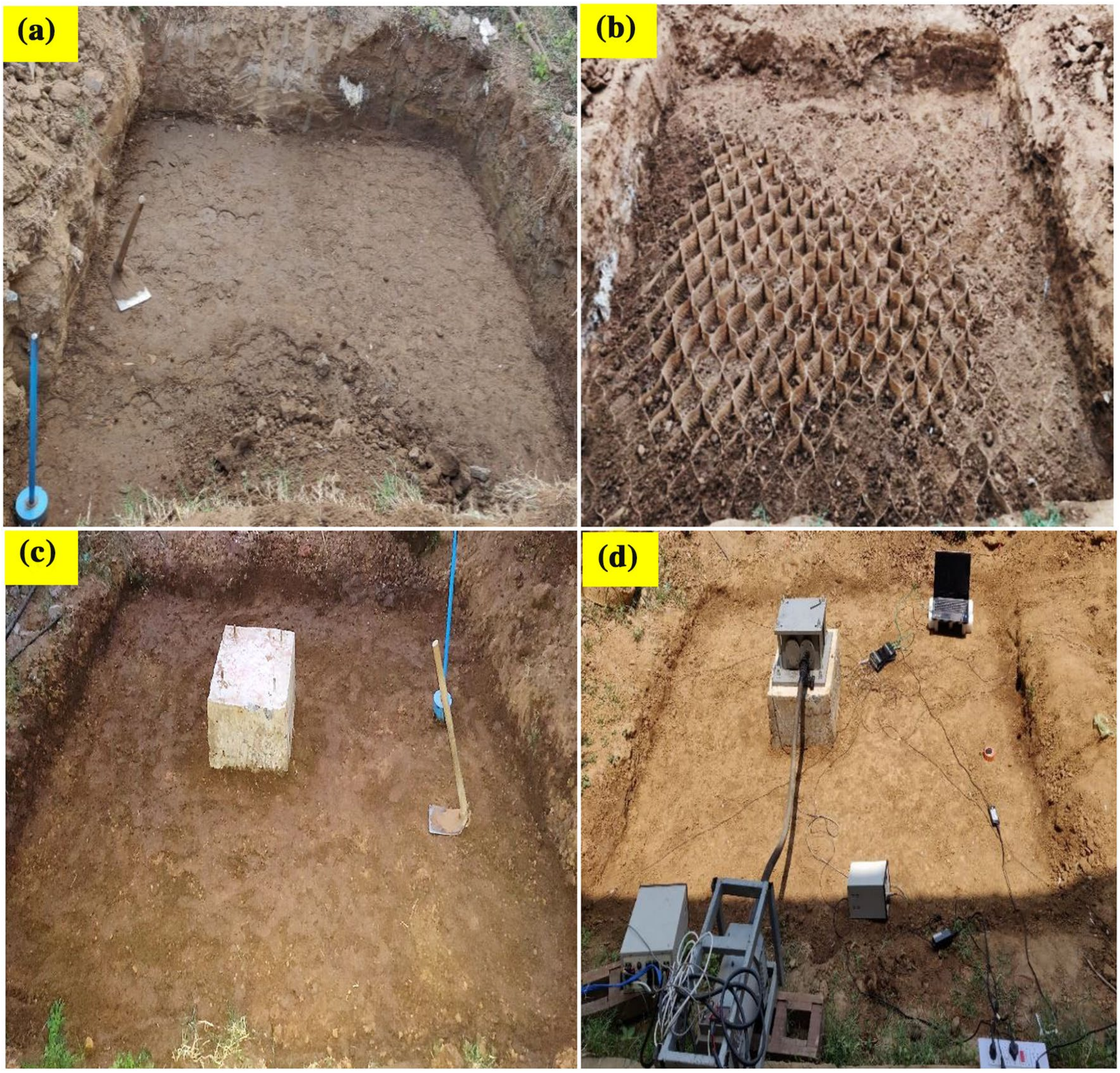

Fig. 3 Foundation bed preparation: **a** partially compacted test bed; **b** partially filled geocell mattress; **c** placement of model footing; and **d** completed test setup

mattress (b) on the vibration mitigation efficacy was studied in GRFB-I. The b was varied from 3 to 6B with an increment of 1B. In GRFB-II, the effect of depth of placement of geocell (μ) was investigated. In this series, geocell was positioned at different locations of 0.1B, 0.3B, and 0.5B under the model footing. The depth of footing embedment (D_f) was varied from 0B to 0.5B in the series of GRFB-III. Whereas, the influence of infill materials on the screening efficiency of the GRFB was studied in the case of GRFB-IV. Four different geo-materials were used to fill the geocell pockets apart from silty sand material. In all the series of experiments, operating frequency (f) was varied from 0 to 45 Hz. Table 3 illustrates the details of the experimental program followed in the present investigation. Overall, 90 numbers of field tests (including repetitive tests) were performed over the unreinforced and geocell reinforced test beds.

Test Procedure

Primarily, accelerometer and geophone positions were marked on the ground surface with respect to the location of model footing. After positioning the footing, the oscillator was fixed to facilitate the loading. The necessary measures were taken to maintain the center of gravity of the footing and the loading system in the same vertical line. The oscillator and DC Motor was properly connected through the flexible shaft to control the extra moments induced over the footing. To overcome the abrupt application of dynamic excitation, the oscillator was run slowly through a speed control unit. The vibration frequency was increased in the increments of 0.5–1 Hz. This process is helpful for the accurate measurement of peak amplitude for various reinforced cases. The dynamic force variation with the increase

Table 3 Overview of field tests

Test series	Contributing parameter	Variable parameters/material	Constant parameters/material
Unreinforced	Depth of embedment of footing	$D_f/B = 0$, 0.25, and 0.5; $\theta = 10°–50°$; $f = 0–45$ Hz	$L/B = 6$; $H/B = 2$; $h/B = 0.2$
GRFB-I	Width of geocell mattress	$b/B = 3$, 4, 5 and 6; $\theta = 10°–50°$; $f = 0–45$ Hz	$\mu/B = 0.1$; silty sand infill; $D_f/B = 0$
GRFB-II	Depth of placement of geocell	$\mu/B = 0.1$, 0.3, and 0.5; $\theta = 10°–50°$; $f = 0–45$ Hz	$b/B = 5$; silty sand infill; $D_f/B = 0$
GRFB-III	Depth of embedment of footing	$D_f/B = 0$, 0.25, and 0.5; $\theta = 10°–50°$; $f = 0–45$ Hz	$\mu/B = 0.1$; $b/B = 5$; silty sand infill
GRFB-IV	Infill material	Sand, steel slag, CDW, and aggregate; $\theta = 10°–50°$; $f = 0–45$ Hz	$\mu/B = 0.1$; $D_f/B = 0$; $b/B = 5$

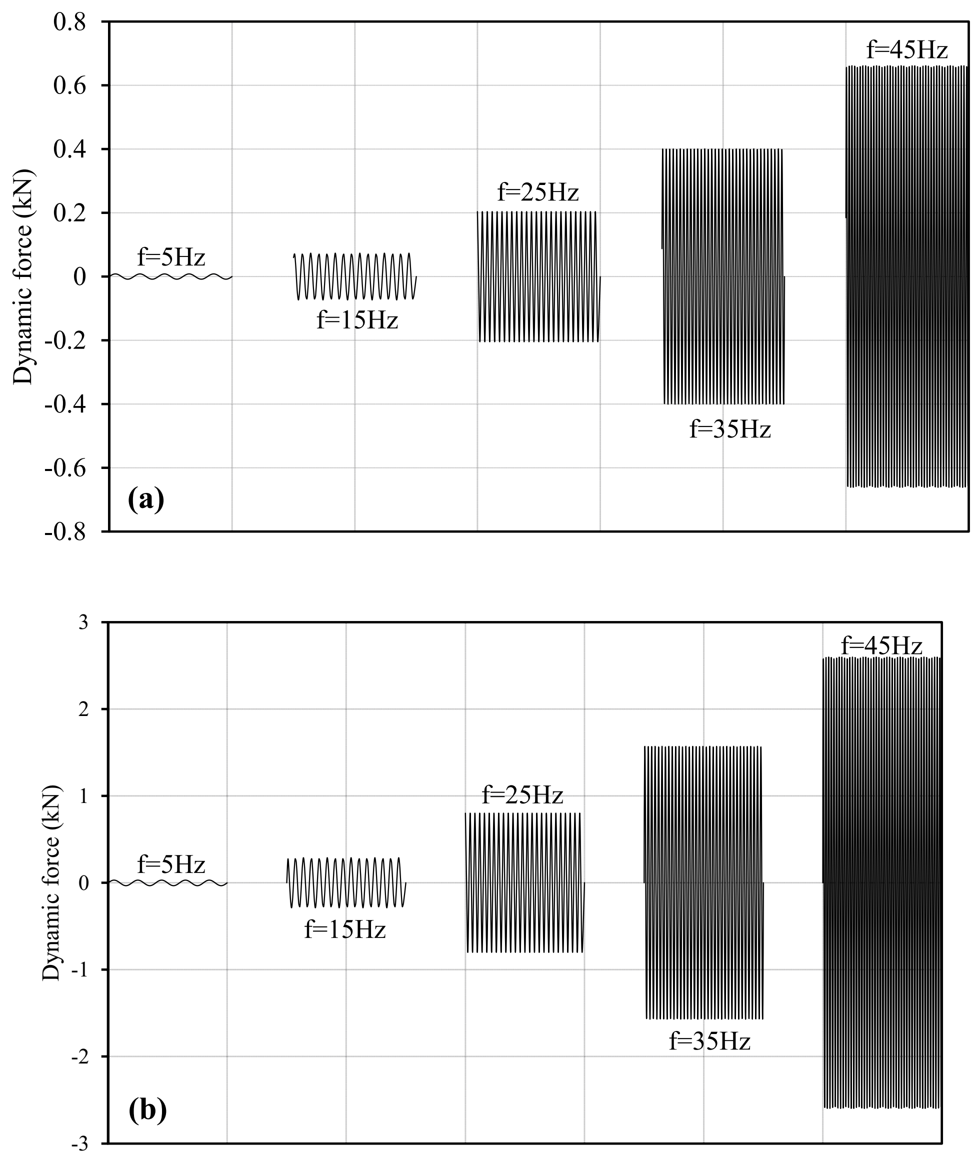

Fig. 4 Variation of dynamic force with operating frequency: **a** 10° eccentric angle; and **b** 40° eccentric angle

in operating frequency at two different eccentric angles is shown in Fig. 4.

Results and Discussion

Effect of the Width of the Geocell Mattress

A typical amplitude versus frequency variation of foundation bed for varying width of the geocell layer is shown in Fig. 5a. The results presented in the figure are pertaining to the eccentric angle of 40°. From the figure, peak displacement amplitude observed in each case represents the resonance condition. Generally, resonance can be observed when the operating frequency of the oscillator matches with the natural frequency of the foundation bed. Thus, the operating frequency associated with the resonance condition is stated as a natural frequency in the remaining portion of the manuscript. In addition, displacement amplitude at the resonance can be referred as resonant amplitude. It was observed that a 36–53% drop in resonant amplitude of foundation bed with the increase in geocell width from 3*B* to 6*B*. Similarly, with the increase in geocell width from 3*B* to 6*B,* 1.35–1.52 times enhancement in the natural frequency of the foundation bed was observed. All-round confinement exerted by geocell makes the reinforced bed stiffer and causes the improvement of natural frequency.

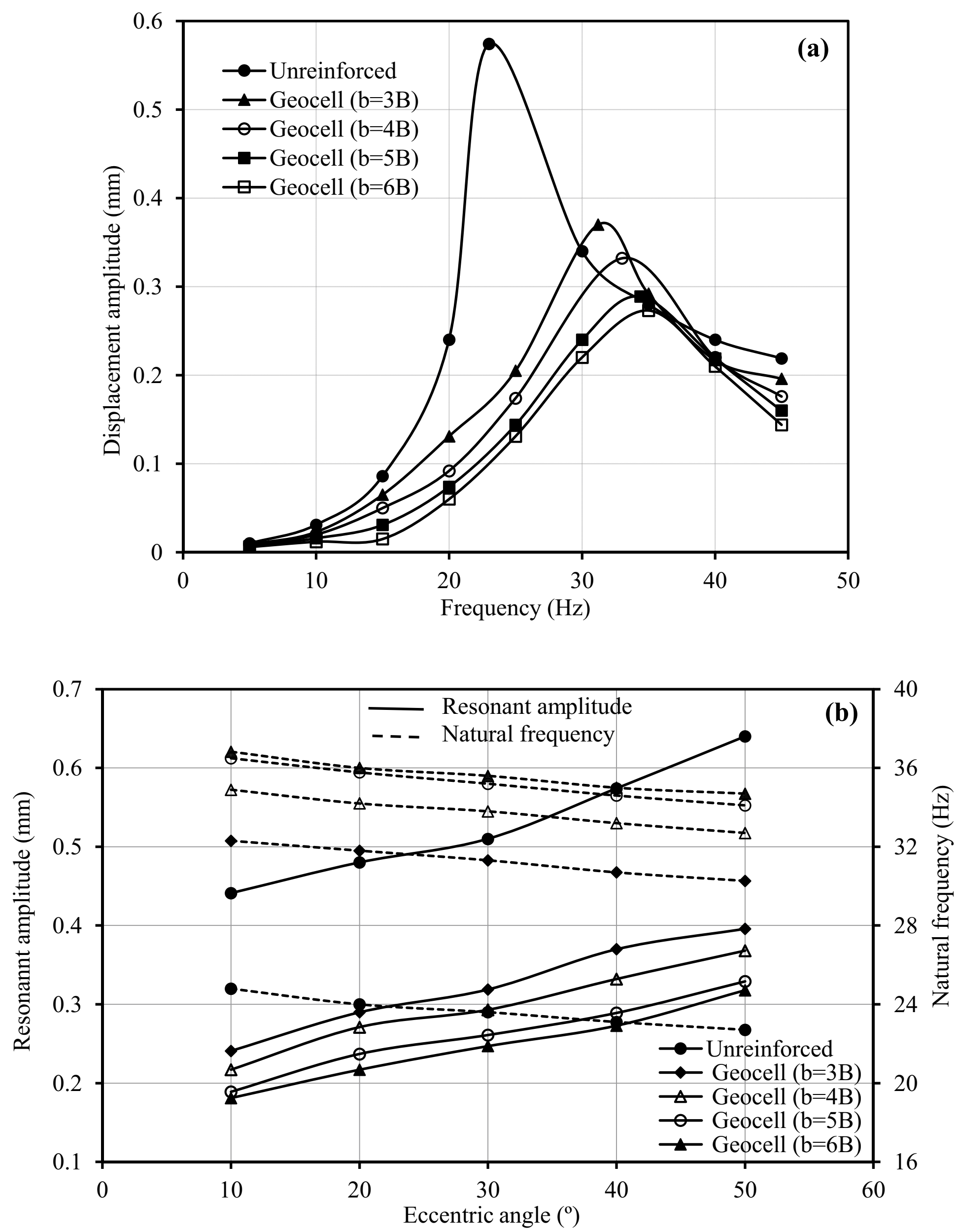

Fig. 5 Influence of width of the geocell mattress on **a** amplitude versus frequency response; and **b** resonance parameters

Figure 5b shows the effect of the eccentric angle (θ) on the resonant amplitude and natural frequency response of the unreinforced and geocell reinforced cases. The increase in θ indicates the increase in the magnitude of dynamic force over the model footing (as per Eq. 2). From the figure, increase in θ resulted in (1) increase in resonant amplitude and (2) a slight drop in the natural frequency of the reinforced beds. The increase in participation of total foundation soil mass in the vibration with the increase in θ was the reason for the reduction in natural frequency. At a particular θ value, the peak displacement amplitude of the GRFB was found smaller than that of the unreinforced bed. Similarly, the higher natural frequency was witnessed in the geocell reinforced case as compared to the unreinforced case. It is worth mentioning that, Kumar and Reddy [44] also reported a similar observation for the unreinforced case based on the experimental results.

One possible reason for the decrease in resonant amplitude of foundation bed in the presence of geocell was due to the increase in stiffness. From Fig. 5a, a single peak displacement amplitude was observed in all the cases with the increase in operating frequency. It indicates that reinforced soil beds behave like a single degree of freedom system (SDFS). Hence, the concept of SDFS was used to understand the stiffness variation of reinforced cases [45].

In this study, the fundamental natural frequency equation was used to describe the stiffness variation of different reinforced cases. Generally, the stiffness of the foundation bed (K) is obtained by,

$$K = 4\pi^2 f_n^2 M \tag{3}$$

where M indicates the total vibrating mass used in the vibration test, and f_n represents the natural frequency of the foundation soil system. As per Eq. 3, K is a dependent parameter of f_n. The f_n can be considered from Fig. 5b. It demonstrates that the GRFB offers more stiffness by virtue of higher f_n value in comparison with the unreinforced condition.

On the other hand, the velocity of soil particles due to the induced vibration was quantified in terms of peak particle velocity (PPV). It is widely used to define the threshold limits and to evaluate the level of risk produced by the induced vibration to the inhabitants and adjacent constructions. Primarily, velocity variation at 2 m distance from the model footing was recorded using a 3D geophone. It measures the velocity response continuously in three orthogonal directions. Finally, PPV is determined using,

$$PPV = \sqrt{(V_x^2 + V_y^2 + V_z^2)} \tag{4}$$

where V_x, V_y, and V_z are the soil particle velocities corresponding to the lateral, longitudinal, and vertical directions respectively. In addition, to measure the acceleration response, six numbers of accelerometers were arranged around the footing (as shown in Fig. 2b). For better comparison, PPV and acceleration were measured at the dynamic excitation corresponds to 30 Hz operating frequency and 40° eccentric angle.

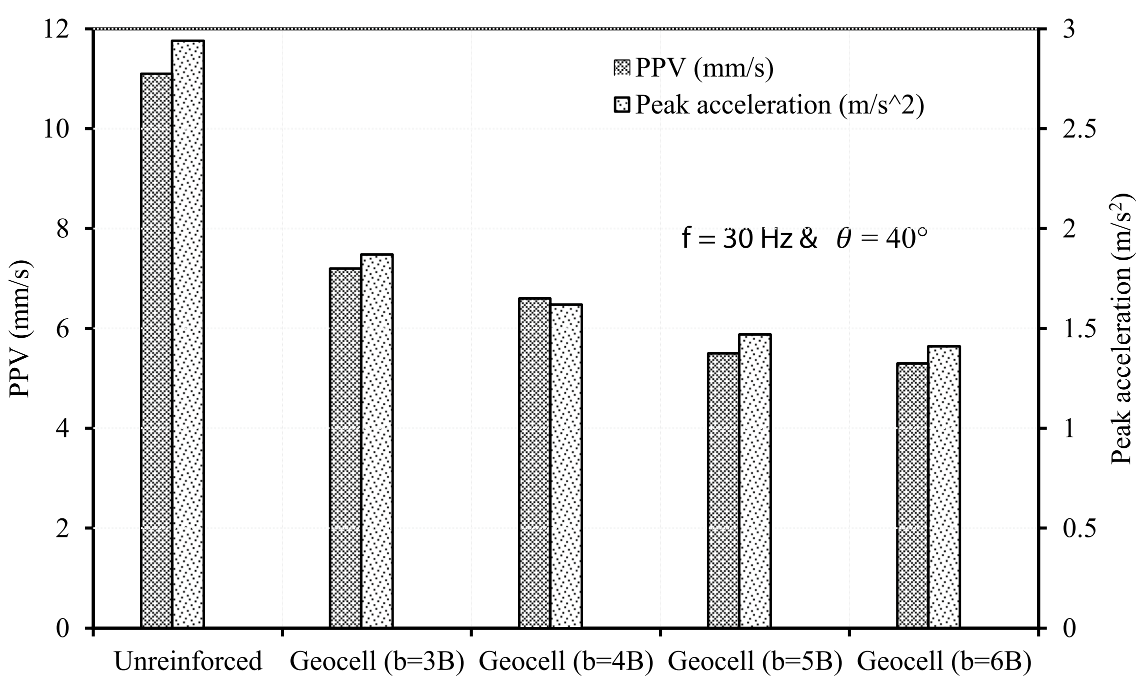

Fig. 6 Effect of geocell width on PPV and peak acceleration of the foundation bed

Figure 6 shows the variation of PPV and peak acceleration with the increase in width of the geocell mattress. The acceleration shown in the figure was the average value observed from all the accelerometers. As the increase in geocell width, reduction in PPV, and acceleration of the vibration was observed. The percentage reduction in both the parameters was noticed minimum beyond the geocell width of 5*B*. Thus, the geocell width of 5*B* was found optimum for the substantial mitigation of the vibration response. At the optimal width, the decrease in acceleration of the foundation bed was noticed by 48%. In addition, 2.2 times improvement in the stiffness of the foundation bed was observed. It is also worth mentioning that the maximum and minimum deviation in the acceleration recorded from the accelerometers was noticed as 9% and 3%, respectively as compared to the average acceleration.

The change in damping behavior of the foundation bed due to the inclusion of geocell might be the probable cause for the reduction in the vibration intensity. Thus, the damping ratio of unreinforced and GRFB cases was calculated from Fig. 5a using the half-power bandwidth method [46, 47]. According to this method, the damping ratio (D_r) of the reinforced soil beds is calculated by,

$$D_r = \frac{f_2 - f_1}{2 \times f_n} \tag{5}$$

where f_n indicates the natural frequency, f_1 and f_2 represents the half-power frequencies. Using Eq. (5), the damping ratio of the unreinforced case was determined as 10.8%. Similarly, 16.2%, 18%, 19.3%, and 19.41% were the D_r values of the GRFB at the geocell widths of 3*B*, 4*B*, 5*B*, and 6*B*, respectively. It highlights the distinct enhancement in the damping behavior of foundation bed by the provision of geocell mattress. Hence, it leads to a considerable reduction in PPV and acceleration.

Effect of Depth of Placement of the Geocell Mattress

Figure 7a demonstrates the variation of displacement amplitude with operating frequency for different depth of placement of geocell. The placement of geocell at the shallow depth below the model footing (i.e. 0.1*B*) leads to (1) a significant reduction in resonant amplitude, and (2) maximum improvement in the natural frequency of the foundation bed. In addition, the rate of reduction in resonant amplitude was found to decrease with the increase in the depth of placement of geocell. It was attributed due to the decrease in stiffness of the GRFB on the account of the increase in depth of placement of geocell. The effect of θ and geocell location on the resonant amplitude and natural frequency variation of GRFB is shown in Fig. 7b. At the geocell location of 0.1*B* (regardless of θ), more than 50% decrement in resonant amplitude of the foundation bed was noticed. Similarly, it was noticed that the 1.47 times increase in the natural frequency of the foundation bed. Nevertheless, natural frequency improvement was decreased to 1.2 times with the change in geocell placement to 0.5*B*. Similarly, the percentage reduction in resonant amplitude was decreased to 21%.

The effect of depth of placement of geocell on PPV and acceleration is shown in Fig. 8. The maximum attenuation of PPV and peak acceleration was also noticed at the shallow depth of placement of the geocell mattress. It indicates that the vibration mitigation is very sensitive to the location of geocell. Hence, 0.1*B* is considered as an optimum geocell placement for the efficient attenuation of vibration parameters. The decrease in damping effect with regards to the increase in geocell location below the footing might be the reason for the amplification of vibration parameters.

Effect of Depth of Embedment of Footing

The effect of footing embedment on the variation of vibration parameters was quantified separately for the unreinforced and geocell reinforced cases. Frequency versus displacement amplitude variation of unreinforced and GRFB with the footing embedment is shown in Fig. 9a. In both cases, increase in footing embedment resulted in the marginal improvement of natural frequency and the significant drop in resonant amplitude. Based on field test results, the resonant amplitude of unreinforced case without the footing embedment was reduced by 16%, and 21%, respectively, at the embedment depths of 0.25*B* and 0.5*B*. Similarly, the resonant amplitude of the GRFB without the embedment was reduced by 17% at 0.25*B* embedment to 24% at 0.5*B* embedment. It reveals that the reduction in resonant amplitude is more substantial at lower values of embedment depth as compared to the higher embedment depths. Further, amplification in the resonant amplitude was noticed with the increase in θ irrespective of the reinforced case and footing embedment as shown in Fig. 9b. On the other hand, from Fig. 9c, at each footing embedment, the natural frequency of both the cases were decreased with the increase in θ.

The effect of footing embedment on the PPV and acceleration was also studied. Figure 10a shows PPV variation with the footing embedment for unreinforced and geocell reinforced cases. In the unreinforced case, PPV was reduced by 11%, and 15%, respectively, at the embedment depths of 0.25*B* and 0.5*B* as compared to without embedment. Similarly, PPV of a geocell reinforced case without the embedment was reduced by more than 14% and 19%, respectively, at the embedment depths of 0.25*B* and 0.5*B*. From Fig. 10b, peak acceleration of the unreinforced case was decreased from 2.84 to 1.38 m/s^2 with the change in footing embedment 0*B* to 0.5*B*. Whereas, with the same variation of footing embedment, the acceleration of GRFB was found to lie

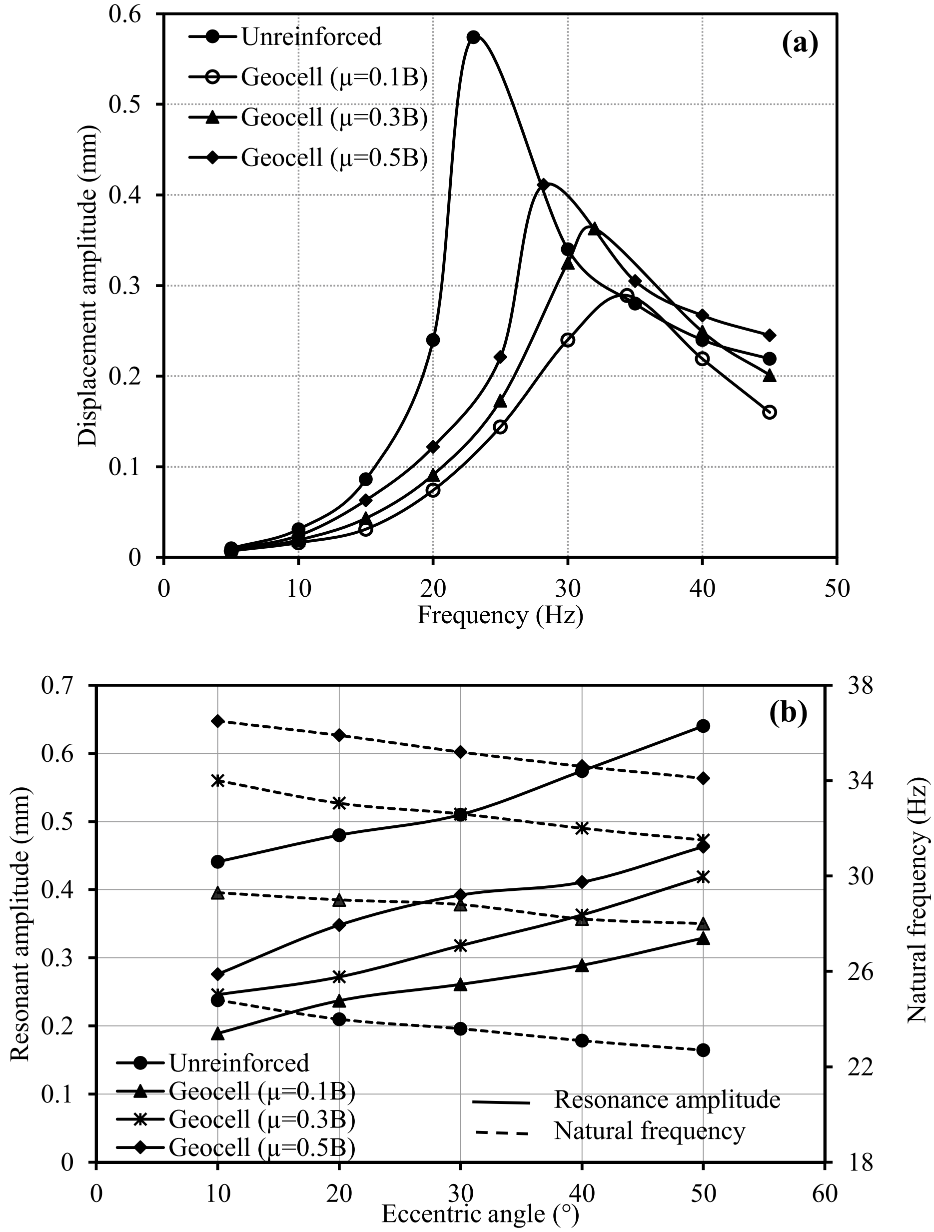

Fig. 7 Effect of depth of placement of geocell on **a** amplitude versus frequency response; and **b** resonance parameters

between 1.48 and 1.08 m/s^2. The improvement in radiation damping with the increase in embedment depth of footing was the reason for the reduction in acceleration and PPV.

Effect of Infill Material

Limited studies reported the increase in performance of GRFB with the change in density and frictional angle of infill material under static and dynamic cases [48, 49]. To examine the influence of infill material on the vibration isolation efficacy, geocell pockets were filled with different geo-materials i.e. silty sand, sand, steel slag, CDW, and aggregate. For convenience, these cases were referred as GSM, GSA, GSS, GCDW, and GAG respectively. The effect of infill material on the resonant amplitude and natural frequency response of the GRFB is shown in Fig. 11. At a particular value of θ, the rate of decrease in resonant amplitude of GRFB was found to increase with the increase in modulus of infill material. Similarly, significant improvement in the natural frequency of GRFB was noticed. Among the considered infill materials, the maximum drop in resonant amplitude was found in the case of aggregate. Similarly, aggregate infill resulted in a higher improvement in the natural frequency of GRFB.

Further, the percentage reduction in PPV of the foundation bed was found to increase with the increase in modulus of infill material as shown in Fig. 12. Table 1 can be referred to find the E value of different geomaterials. Interestingly,

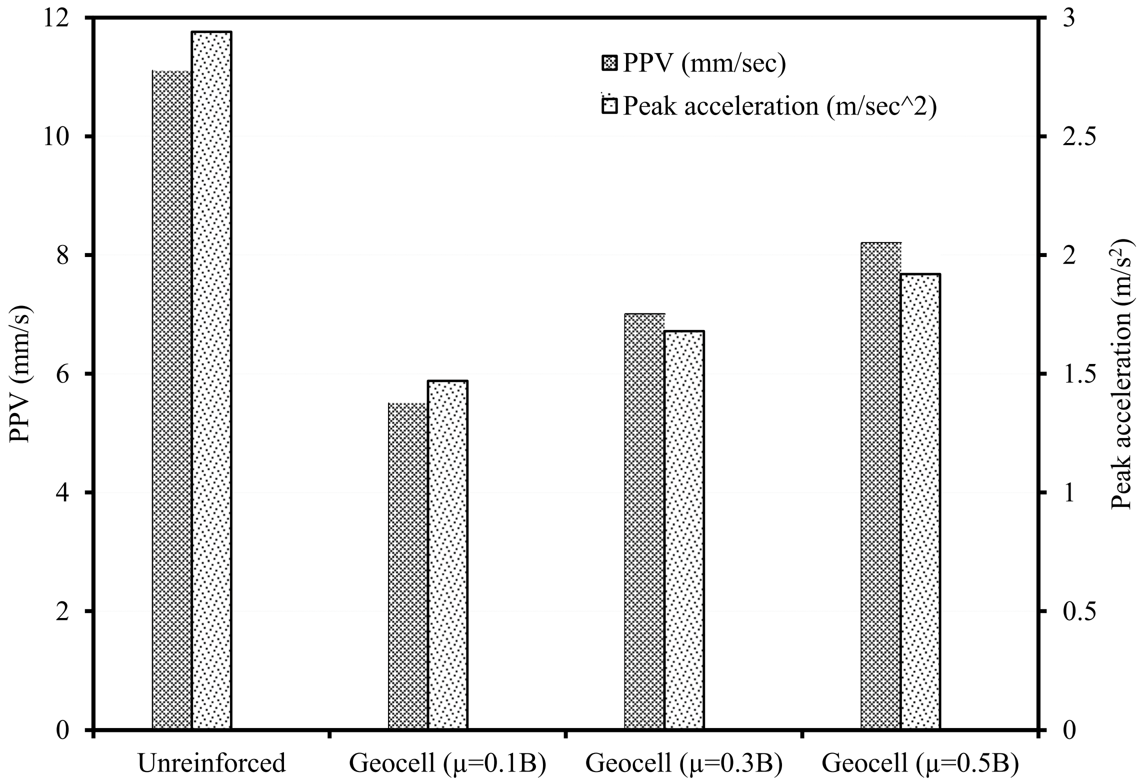

Fig. 8 PPV and acceleration response of foundation bed with the change in depth of placement of geocell reinforcement

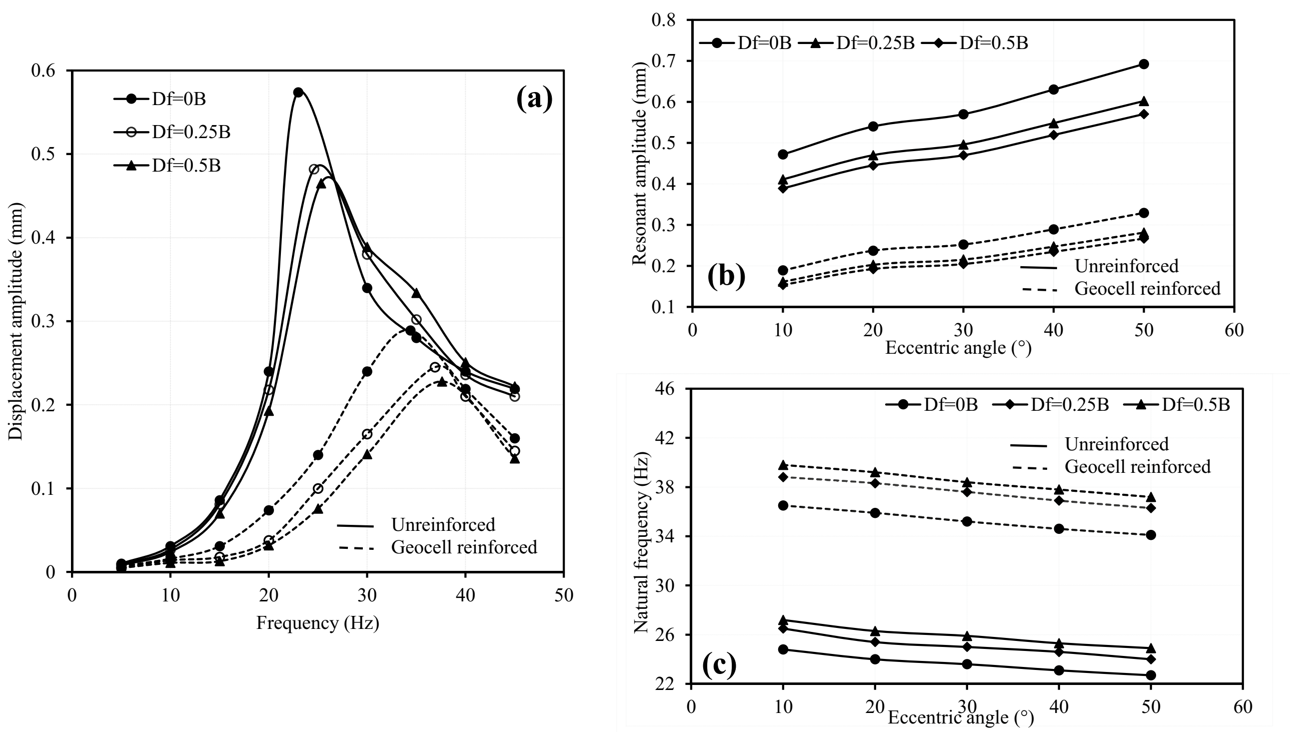

Fig. 9 Effect of depth of embedment of footing on: **a** amplitude versus frequency, **b** resonant amplitude, and **c** natural frequency response of reinforced cases

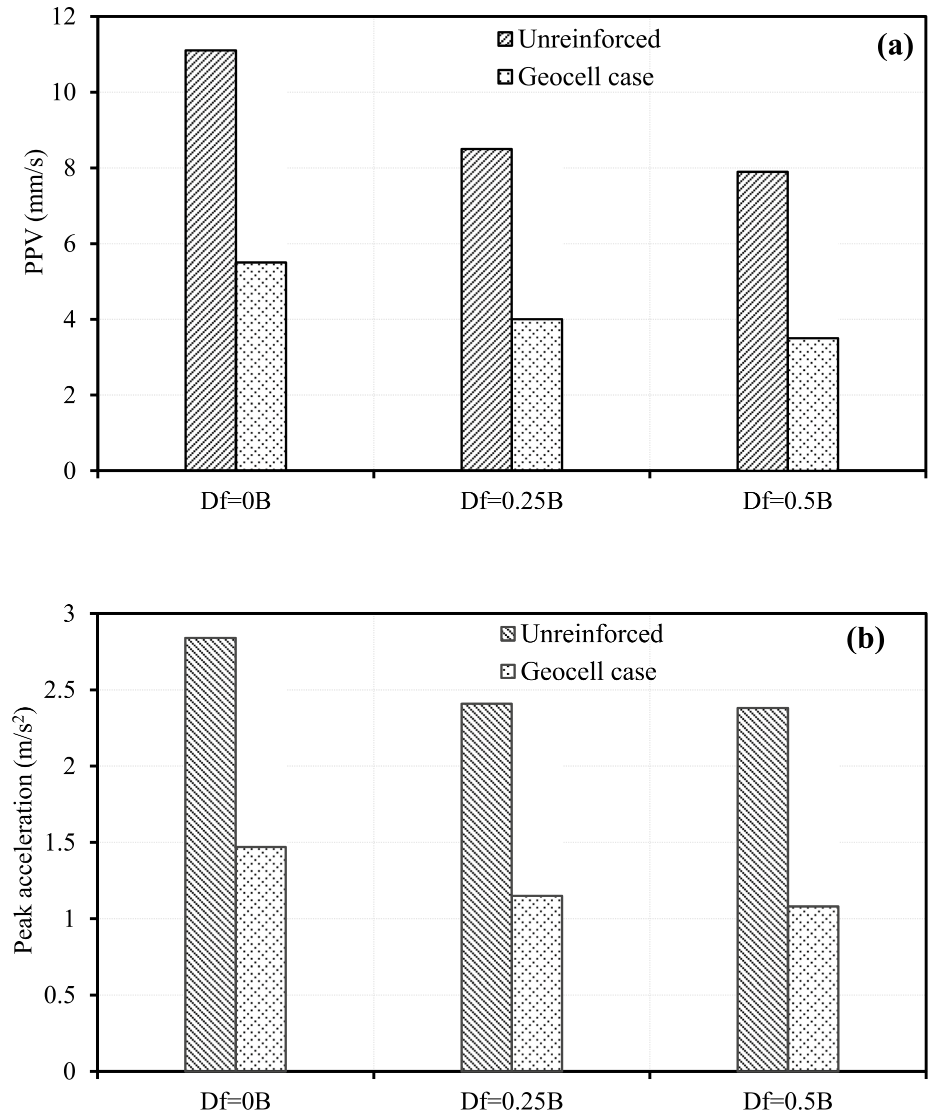

Fig. 10 Change in vibration parameters with the depth of embedment of footing: **a** PPV; and **b** peak acceleration

vibration mitigation efficacy of slag and CDW materials was found higher than the sand infill. Overall, PPV of the foundation bed has attenuated a maximum of 58% by filling the geocell pockets with the aggregate material.

On the other hand, the attenuation rate of acceleration was also found to increase with the increase in modulus of infill material. The typical acceleration versus time response of the unreinforced and geocell infilled cases is shown in Fig. 13a–f. The maximum increase in the damping ratio of the GRFB in the case of aggregate was the reason for the high percentage reduction of PPV and acceleration as compared to other cases.

Conclusions

In this study, a field investigation was undertaken to investigate the effect of numerous key parameters on the vibration isolation efficacy of geocell reinforced beds. It includes the width of the geocell mattress, depth of placement of geocell below the footing, depth of embedment of footing, and infill material. The effect of each influencing parameter on the vibration isolation efficacy of GRFB was highlighted.

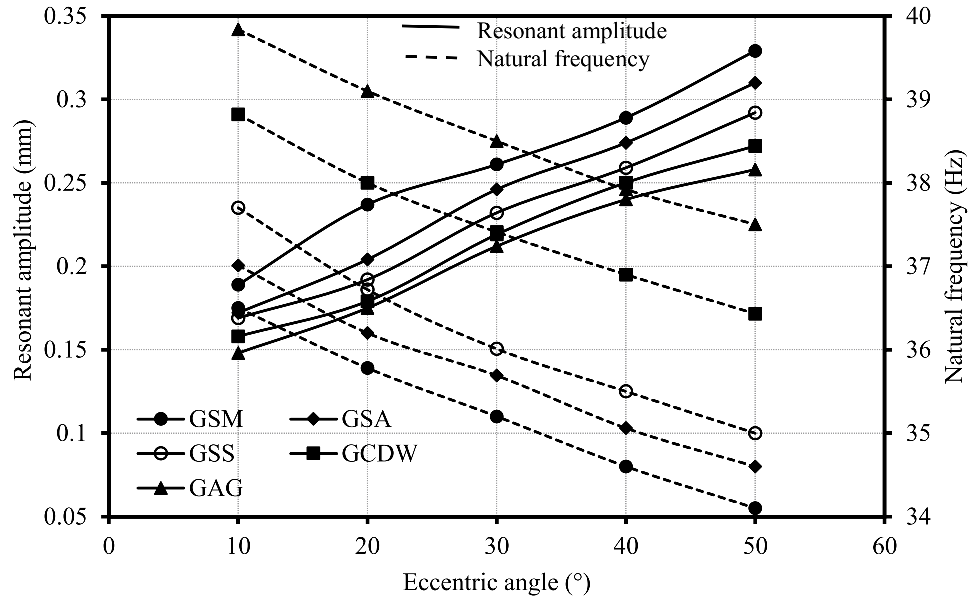

Fig. 11 Influence of infill material on the resonance parameters of GRFB

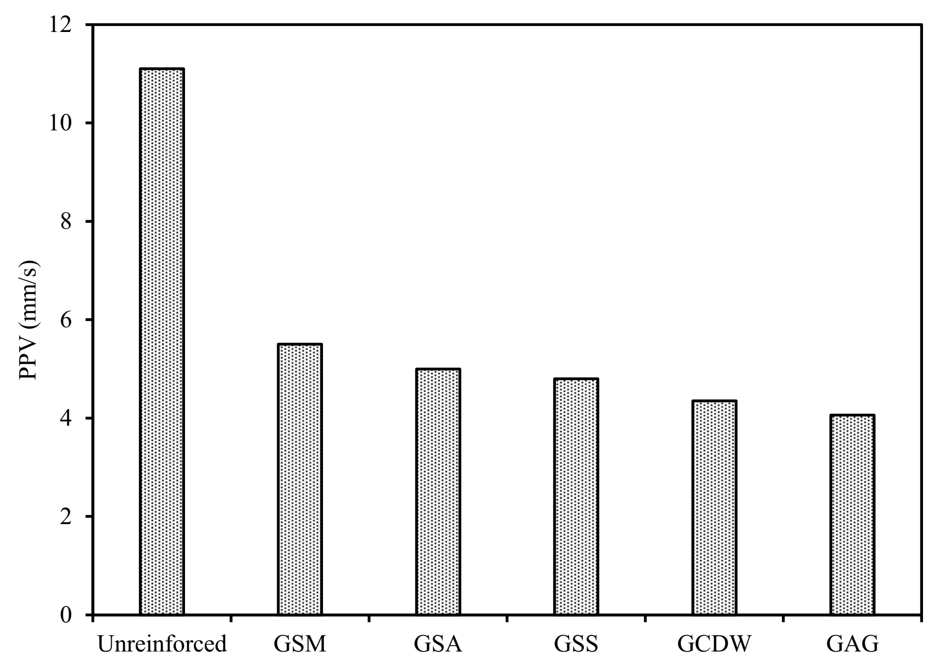

Fig. 12 Influence of infill material on PPV response of GRFB

- Based on the field test results, the isolation efficacy of GRFB was enhanced with the increase in width of geocell and minimizing the depth of placement of the geocell below the footing. For the effective vibration isolation, optimum width and depth of placement of geocell were observed as 5*B* and 0.1*B*, respectively.
- At the optimum parameters, 2.2 times improvement in the stiffness of the foundation bed was observed. As a result, more than 50% reduction in resonant amplitude and 1.46 times improvement in natural frequency was observed.
- Further, the damping ratio of the GRFB was increased by 76% as compared to the unreinforced case. It caused a substantial decrement in peak acceleration and PPV of the foundation bed.
- Thereafter, the increase in footing embedment resulted in a notable decrease in resonant amplitude and a slight improvement in the natural frequency of the unreinforced and GRFB. The reduction rate of PPV and acceleration was found marginal beyond the embedment depth of 0.25*B*. Hence, the embedment depth of footing is sug-

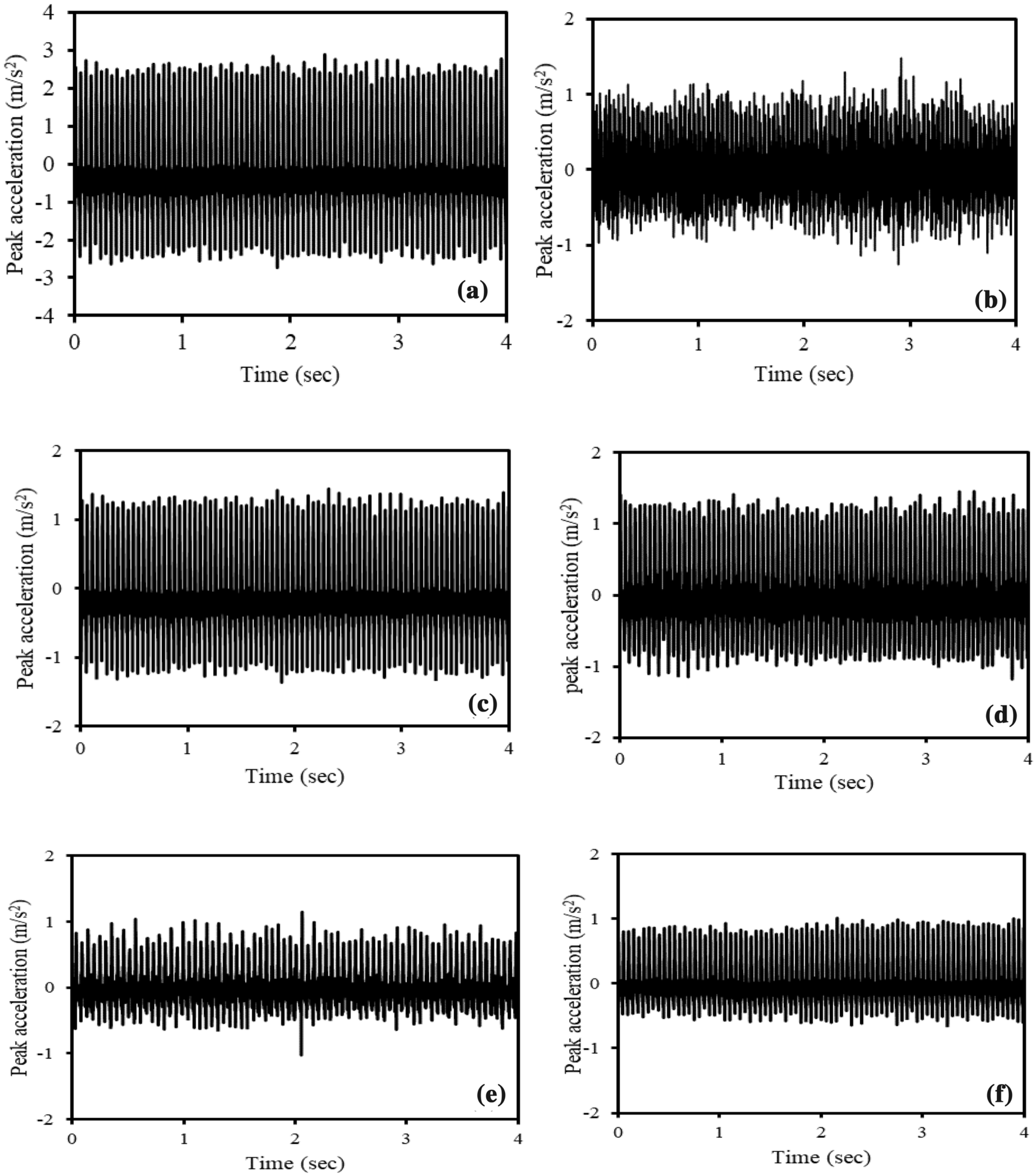

Fig. 13 Acceleration—time histories of **a** unreinforced; **b** GSM; **c** GSA; **d** GSS; **e** GCDW; and **f** GAG cases

gested as $0.25B$ for the better mitigation of vibration parameters.

- The attenuation rate of vibration indicators was found to increase with the increase in modulus of infill material. The percentage reduction in PPV and peak acceleration was observed maximum in the GAG case.
- Nevertheless, the increase in the eccentric angle caused the amplification of resonant amplitude and the drop in the natural frequency of GRFB and unreinforced cases.

References

1. Bose T, Choudhury D, Sprengel J, Ziegler M (2018) Efficiency of open and infill trenches in mitigating ground-borne vibrations. J Geotech Geoenviron Eng 144(8):04018048
2. Kattis SE, Polyzos D, Beskos DE (1999) Vibration isolation by a row of piles using a 3-D frequency domain BEM. Int J Numer Meth Eng 46(5):713–728
3. Massarsch KR (2005) Vibration isolation using gas-filled cushions. In: Woods RD (ed) Soil dynamics symposium in honor of professor. Proceedings of the Geo-Frontiers Congress, American Society of Civil Engineers, January 24–26, Austin, Texas, USA, pp 1–20
4. Murillo C, Thorel L, Caicedo B (2009) Ground vibration isolation with geofoam barriers: centrifuge modeling. Geotext Geomembr 27(6):423–434
5. Ulgen D, Toygar O (2015) Screening effectiveness of open and in-filled wave barriers: a full-scale experimental study. Constr Build Mater 86:12–20
6. Jayawardana P, Thambiratnam DP, Perera N, Chan T (2019) Dual in-filled trenches for vibration mitigation and their predictions using artificial neural network. Soil Dyn Earthq Eng 122:107–115
7. Takemiya H (2004) Field vibration mitigation by honeycomb WIB for pile foundations of a high-speed train viaduct. Soil Dyn Earthq Eng 24(1):69–87
8. Gao GY, Feng SJ, Li W, Zheng JG (2007) 2-D analysis of vibration isolation by wave impeding block in layered ground. J Vib Eng 20(2):174–179
9. Tsai PH, Feng ZY, Jen TL (2008) Three-dimensional analysis of the screening effectiveness of hollow pile barriers for foundation-induced vertical vibration. Comput Geotech 35(3):489–499
10. Xu M, Wang X, Min C (2011) Vibration reduction due to wave impedance block embedded in layered elastic soil with BEM transfer matrix method. J Nanchang Inst Technol 30(3):21–26
11. Gao G, Chen J, Gu X, Song J, Li S, Li N (2017) Numerical study on the active vibration isolation by wave impeding block in saturated soils under vertical loading. Soil Dyn Earthq Eng 93:99–112
12. Kratzig WB, Niemann HJ (1996) Dynamics of civil engineering structures. Balkema, Rotterndan, pp 466–484
13. Takemiya H (2009) Field tests of PCA-WIB with tire shreds fill-in for vibration mitigation. In: Proceedings of the 4th international symposium on environmental vibrations-prediction, monitoring, mitigation and evaluation. Beijing, pp 254–259
14. Mandal A, Baidya DK, Roy D (2012) Dynamic response of the foundations resting on a two-layered soil underlain by a rigid layer. Geotech Geol Eng 30(4):775–786
15. Rajesh S, Viswanadham BVS (2012) Centrifuge model studies on the performance of geogrid reinforced soil barriers of landfill covers. Indian J Geosynth Ground Improv 1(1):20–28
16. Obando-Ante J, Palmeira EM (2015) A laboratory study on the performance of geosynthetic reinforced asphalt overlays. Int J Geosynth Ground Eng 1(1):5
17. Boominathan S, Senathipathi K, Jayaprakasam V (1991) Field studies on dynamic properties of reinforced earth. Soil Dyn Earthq Eng 10(8):402–406
18. Jha JN, Shukla SK (2015) Bearing capacity and settlement characteristics of sand subgrades with vertical reinforcement supporting a square footing. Int J Geosynth Ground Eng 1(2):16
19. Vangla P, Latha GM (2015) Influence of particle size on the friction and interfacial shear strength of sands of similar morphology. Int J Geosynth Ground Eng 1(1):6
20. Yoo C, Lee D (2012) Performance of geogrid-encased stone columns in soft ground: full-scale load tests. Geosynth Int 19(6):480–490
21. Saride S, Dutta TT (2016) Effect of fly-ash stabilization on stiffness modulus degradation of expansive clays. J Mater Civ Eng 28(12):04016166
22. Haldar S, Sivakumar Babu GL (2009) Improvement of machine foundations using reinforcement. Proc Inst Civ Eng-Ground Improv 162(4):199–204
23. Muthukumar S, Sakthivelu A, Shanmugasundaram K, Mahendran N, Ravichandran V (2019) Performance assessment of square footing on jute geocell-reinforced sand. Int J Geosynth Ground Eng 5(3):25
24. Satyal SR, Leshchinsky B, Han J, Neupane M (2018) Use of cellular confinement for improved railway performance on soft subgrades. Geotext Geomembr 46(2):190–205
25. Song F, Liu H, Hu H, Xie Y (2018) Centrifuge tests of geocell-reinforced retaining walls at limit equilibrium. J Geotech Geoenviron Eng 144(3):1–13
26. Dash SK, Choudhary AK (2018) Geocell reinforcement for performance improvement of vertical plate anchors in sand. Geotext Geomembr 46(2):214–225
27. Shadmand A, Ghazavi M, Ganjian N (2018) Load-settlement characteristics of large-scale square footing on sand reinforced with opening geocell reinforcement. Geotext Geomembr 46(3):319–326
28. Nadaf MB, Mandal JN (2017) Numerical analyses of loaded strip footing resting on cellular mattress and strips: reinforced fly ash slope. Int J Geosynth Ground Eng 3(3):26
29. Hegde A (2017) Geocell reinforced foundation beds-past findings, present trends and future prospects: a state-of-the-art review. Constr Build Mater 154:658–674
30. Sherin KS, Chandrakaran S, Sankar N (2017) Effect of geocell geometry and multi-layer system on the performance of geocell reinforced sand under a square footing. Int J Geosynth Ground Eng 3(3):20
31. Suku L, Prabhu SS, Ramesh P, Babu GS (2016) Behavior of geocell-reinforced granular base under repeated loading. Transp Geotech 9:17–30
32. Latha GM, Manju GS (2016) Seismic response of geocell retaining walls through shaking table tests. Int J Geosynth Ground Eng 2(1):7
33. Venkateswarlu H, Ujjawal KN, Hegde A (2018) Laboratory and numerical investigation of machine foundations reinforced with geogrids and geocells. Geotext Geomembr 46(6):882–896
34. Ujjawal KN, Venkateswarlu H, Hegde A (2019) Vibration isolation using 3D cellular confinement system: a numerical investigation. Soil Dyn Earthq Eng 119:220–234
35. ASTM D698–07 (2012) Standard test methods for laboratory compaction characteristics of soil using standard effort (12,400 ft-lbf/ft^3 (600 kN-m/m^3)). ASTM International, West Conshohocken
36. ASTM D4253–16 (2016) Standard test method for minimum index density and unit weight of soils and calculation of relative density. ASTM international, West Conshohocken
37. ASTM D3080–4 (2004) Standard test method for direct shear test of soils under consolidated drained conditions. ASTM International, West Conshohocken
38. ISO, E. 10319 (2015) Geotextiles, wide width tensile test. Comité Européen de Normalisation, Brussels
39. Richart FE, Hall JR, Woods RD (1970) Vibration of soils and foundations. Int Ser Theor Appl Mech XViii:1–414
40. Mehrjardi GT, Behrad R, Tafreshi SM (2019) Scale effect on the behavior of geocell-reinforced soil. Geotext Geomembr 47(2):154–163
41. Biswas A, Krishna AM (2017) Geocell-reinforced foundation systems: a critical review. Int J Geosynth Ground Eng 3(2):17

42. IS. 2720–29 (1975) Methods of test for soil—part XXIX: determination of dry density of soils in-place. Prabhat Offset Press, Delhi, pp 4–8
43. Hegde A, Sitharam TG (2015) 3-Dimensional numerical modelling of geocell reinforced sand beds. Geotext Geomembr 43(2):171–181
44. Kumar J, Reddy CO (2006) Dynamic response of footing and machine with spring mounting base. Geotech Geol Eng 24(1):15–27
45. Bharathi M, Dubey RN (2018) Dynamic lateral response of under-reamed vertical and batter piles. Constr Build Mater 158:910–920
46. Blake RE (1961) Basic vibration theory. Shock Vib Handb 1:2–8
47. Venkateswarlu H, Hegde A (2019) Block resonance test on geosynthetic reinforced foundation beds. In: Meehan CL, Kumar S, Pando MA, Coe JT (eds) Geo-congress 2019: earth retaining structures and geosynthetics. American Society of Civil Engineers, Reston, pp 266–276
48. Tafreshi SM, Zarei SE and Soltanpour Y (2008) Cyclic loading on foundation to evaluate the coefficient of elastic uniform compression of sand. In: The 14th world conference on earthquake engineering, Beijing
49. Hegde AM, Sitharam TG (2015) Effect of infill materials on the performance of geocell reinforced soft clay beds. Geomech Geoengin 10(3):163–173